



OPEN

# A case study of displacement, stress condition and failure criterion of surrounding rock in deep super-large section double chambers in the Longgu Coal Mine, Shandong, China

Zihui Wang<sup>1,2</sup>, Shuo Zhang<sup>2</sup>, Deyuan Fan<sup>1,2</sup> & Dongxiao Zhang<sup>2</sup>✉

To investigate the stability of a super-large section chamber group, an analysis was conducted based on the in-situ geological conditions of a super-large section chamber group utilized as a coal gangue separation system at the Longgu Coal Mine. Field measurement and numerical simulation were employed to analyze the failure area and stress state of the surrounding rock under varying chamber spacings. The results indicate that the extent of the plastic zone significantly expands when the spacing between chambers is less than 2.0 times the chamber width. When the distance between chambers is 1.5 times the chamber width, it results in the rock pillars being entirely within the plastic zone. As the chamber spacing decreases, the tangential stress within the rock pillar range increases. When the chamber spacing is 2.5, 2.0, and 1.5 times the chamber width, the maximum tangential stress is 1.19, 1.46, and 1.18 times that in the case of a single chamber, respectively. Based on the displacement analysis, it was observed that as the distance between the chambers decreases, there is a notable increase in the displacement of the pillar sides and chamber top, indicating a higher risk of collapse. Integrating the plastic area and stress analysis allows for the categorization of the rock pillar area into four sections: the broken area, loose area, stable area, and firm area. Drawing upon the theoretical solution of the plastic zone of a circular chamber and the equivalent radius method, an approximate solution for the plastic zone of a non-circular chamber has been provided. Furthermore, the minimum reasonable spacing between chambers in a super-large section chamber group is provided as a distance criterion for the failure of a double chamber.

In recent years, with the advancement of mining, water conservancy, and hydropower projects, the size of underground chambers has progressively increased, leading to a rise in complexity in the spatial structure of chambers. Considering the rapid progress of mines towards extensive and intelligent development, numerous super large cross-section chambers and chamber clusters have been established underground in coal mines<sup>1-4</sup>. As the mining depth increases, the geological conditions characterized by “three highs and one disturbance” (high stress, high permeability, high temperature, excavation disturbance) can potentially induce alterations in the organizational structure and fundamental mechanical properties, and engineering response of rocks, which is one of the main reasons for the frequent occurrence of deep engineering disasters around the world<sup>5-7</sup>. The surrounding rock of the tunnel is exposed to more intricate geological conditions, leading to varied engineering responses<sup>8,9</sup>. The stability issue concerning the surrounding rock of super large section tunnel groups is expected to intensify. Furthermore, designating a tunnel as super large based solely on its size is not a straightforward task. Rather than focusing on a single factor, a thorough evaluation should be performed based on indicators such as

<sup>1</sup>State Key Laboratory of Mining Disaster Prevention and Control Cofounded By Shandong Province and the Ministry of Science and Technology, Shandong University of Science and Technology, Qingdao 266590, Shandong, China. <sup>2</sup>College of Energy and Mining Engineering, Shandong University of Science and Technology, Qingdao 266590, Shandong, China. ✉email: 1290763952@qq.com

tunnel burial depth, section area, uniaxial compressive strength, and surrounding rock integrity<sup>10</sup>. Hence, it is essential to investigate the stress state and surrounding rock deformation of the tunnel group post-excitation, as well as establish a failure criterion for the tunnel group that aligns with engineering requirements.

Prior to effectively managing and offering appropriate support for the near-field surrounding rock of super large section chambers, it is crucial to have a comprehensive understanding of their stress state. Domestic and foreign researchers have conducted numerous studies and research projects related to this field. Wang et al.<sup>11</sup> uncovered the progressive law of stress and deformation range of surrounding rock leading up to engineering catastrophe evolution, from an energy perspective. Based on energy analyses, Deng et al.<sup>12</sup> developed a theoretical model and introduced a dimensionless energy parameter to quantitatively characterize the threshold conditions of various types of fault slip events. There exist precise analytical solutions for calculating the stress state and displacement of the near-field surrounding rock of circular tunnels in elastic, viscoelastic, and elastic–plastic media<sup>13–15</sup>. For other shapes of chambers, approximate solutions can be obtained using the complex function method<sup>16–18</sup>. Zhang et al.<sup>19</sup> utilized the Schwarz alternating method to derive iterative solutions for the stress field of chambers with varying numbers, shapes, and layouts. Through the analysis of analytical results, certain regularities can be discerned, offering valuable guidance for addressing practical engineering challenges.

In the study of deformation and failure range of super large section chambers, Wang et al.<sup>20,21</sup> and Wen et al.<sup>22</sup> have developed a structural model for a large mining area. It has been indicated that the deformation and failure process of the surrounding rock of a super large cross-section chamber is prolonged, leading to convergence instability, a wide range of cracks, and stress redistribution. Fan et al.<sup>23</sup> conducted an analysis on the stress and failure evolution of intersections varying in crossing angles and equivalent angular bisectors. And the plastic radius of a super-large section chamber under unequal pressure was adjusted by accounting for the size effect. Liu et al.<sup>24</sup> developed an instability mechanical model for surrounding rock controlled by chamber spacing, and theoretically derived the minimum spacing required to prevent chain instability based on elastoplastic mechanics theory. Xie et al.<sup>25</sup> investigated the deformation of large-scale variable cross-section roadways in deep soft rock. Their study revealed that the roadway deformation exhibits a progressive increase from smaller to larger cross-sections, nearly doubling at the largest cross-section. The plastic zone tends to concentrate at the top plate and shoulder, gradually decreasing from the sides to the bottom corner. Researchers performed statistical analysis on 18 underground chamber groups within the water conservancy and hydropower system. They discovered that the rock mass thickness between two chambers should typically be at least 1–1.5 times the average excavation width of adjacent chambers. Furthermore, the instability mechanism of local nearly horizontal strata in super-large section and deep-buried tunnels was elucidated through the analysis of macro failure and microfracture<sup>26</sup>. Jiang et al.<sup>27</sup> conducted calculations to determine the relationship between the rock column thickness ( $L$ ) and the maximum excavation span ( $B$ ) and height ( $H$ ) of chambers. Their findings indicated that  $L/B$  ranged from 0.60 to 1.80, with about half of the chamber groups exhibiting  $L/B$  values between 1.00 and 1.50, while  $L/H$  ratios varied from 0.35 to 0.80. Numerical simulations<sup>28,29</sup> and similar simulation experiments<sup>30</sup> have also been widely applied in the study of group tunnel effects. Qi et al.<sup>31</sup> utilized FLAC3D to investigate different chamber layouts and achieved stable chamber group structures. Lin et al.<sup>32</sup> examined the reasons for deformation in large section caverns within complex geological settings through a blend of numerical simulations and field measurements. Li et al.<sup>33,34</sup> leveraging a mix of numerical simulations and field data, scrutinized the instability mechanism of surrounding rock in soft rock chambers under high stress conditions, and suggested a approach for enhancing the stability of the rock surrounding soft rock chambers. The research mentioned offers substantial backing for managing the near-field surrounding rocks in super large section chamber groups. Yet, the stress state and failure mechanism of the surrounding rocks in super large section chamber groups remain ambiguous and necessitate additional investigation.

The article is centered on the geological conditions of the super large section chamber group within the underground coal gangue separation system of Shandong Xinjulong Energy Co., Ltd. Through a combination of on-site measurements and numerical simulations, the stress state, deformation characteristics, plastic zone failure range, and the interaction between adjacent chambers post-excitation are thoroughly examined. Furthermore, leveraging elastic–plastic theory, the study delves into the minimum failure spacing of the super large section chamber group in the mine, thereby offering theoretical insights for the stability control of the surrounding rock within the mine chamber group.

## Engineering geological example

### Overview of the mine

The Longgu Coal Mine operated by Xinjulong Energy Company is situated in Heze City, Shandong Province, and falls under the administrative jurisdiction of Longgu Town in Juye County. Notably, the geological reserves of the Longgu Coal Mine are estimated to be about 1.683 billion tons, with a designed production capacity of around 6 million tons per year. Furthermore, the mine boasts a planned service life spanning 82 years, aligning with long-term sustainability and operational objectives.

The coal gangue separation system in the Longgu Coal Mine comprises four significant chambers, namely the screening crushing chamber (SCC), screening product transferring chamber (SPTC), dense medium shallow groove separation chamber (DSSC), and slime water and medium chamber (SWMC), as illustrated in Fig. 1. Situated in a triangular zone delineated by the north main haulage roadway, No. 1 district rise, and No. 1301 mining area, this system operates within the confines of the No. 3 coal seam. The coal is found at depths ranging from 778.6 to 848.6 m, with an average depth of 813.6 m. The primary coal types prevalent in the Longgu coal field's No. 3 coal seam are fat coal and coking coal, characterized by high quality attributes such as low ash, sulfur, phosphorus content, and a high calorific value. The stratigraphic arrangement of the coal seam, alongside the roof and floor strata, is depicted in Fig. 2.

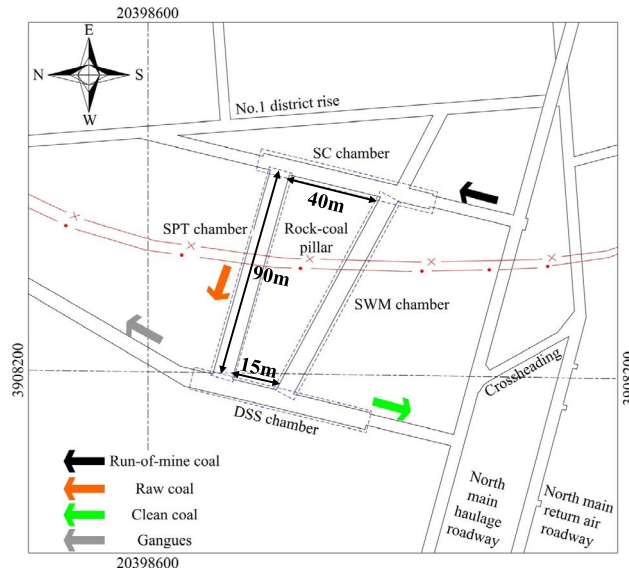


**Figure 1.** Layout of chamber group in coal gangue separation system<sup>28</sup>.

Column	No.	Lithology	Thickness/m	Petrographic description
	1	Siltstone	12.4 ~ 20.2 16.3	Dark gray, horizontal bedding development, uneven fracture
	2	Mudstone	5.3 ~ 11.1 8.2	Grey green, argillaceous and layer structure, ripple bedding fracture
	3	Fine sandstone	2.5 ~ 6.3 4.4	Dark gray, fine-grained round structure, intermittent wavy bedding development
	4	Siltstone	2.0 ~ 6.0 4.0	Dark gray, vertical bedding development, uneven fracture
	5	Fine sandstone	3.8 ~ 4.4 4.1	Dark gray, fine-grained round structure, intermittent wavy bedding development
	6	Siltstone	6.3 ~ 10.7 8.5	Dark gray, vertical bedding development, uneven fracture
	7	Mudstone	5.6 ~ 9.0 7.3	Grey green, argillaceous and layer structure, ripple bedding fracture
	8	Fine sandstone	4.2 ~ 6.2 5.2	Dark gray, fine-grained round structure, intermittent wavy bedding development
	9	Siltstone	2.7 ~ 10.5 6.6	Dark gray, vertical bedding development, uneven fracture
	10	3 coal	3.2 ~ 6.8 5.0	Black, strip and layer structure, dull luster
	11	Siltstone	3.6 ~ 6.2 4.9	Dark gray, vertical bedding development, uneven fracture
	12	Fine sandstone	1.2 ~ 3.4 2.3	Gray, muddy cementation, with small interlaced and gentle-wave bedding
	13	Middle sandstone	5.2 ~ 11.0 8.1	Uniform bedding, muddy filling cracks, semi-hardness
	14	Fine sandstone	3.8 ~ 5.6 4.7	Gray, muddy cementation, with small interlaced and gentle-wave bedding
	15	Siltstone	7.2 ~ 9.4 8.4	Dark gray, vertical bedding development, uneven fracture
	16	Mudstone	9.6 ~ 14.8 12.2	Grey green, argillaceous and layer structure, ripple bedding fracture

**Figure 2.** Lithologic comprehensive histogram in chamber group region<sup>28</sup>.

The description highlights the significant variation in cross-section dimensions across tunnels within the cave group, with the DSSC boasting the largest net cross-sectional area of 104.25 m<sup>2</sup> and the SPTC featuring a net cross-sectional area of 62 m<sup>2</sup>. Additionally, the narrow spacing between tunnels ranging from a minimum of 15 m to a maximum of about 90 m characterizes this as a group of super large cross-section tunnels.

The completion and operationalization of the cave group in late 2013 indicate a commendable overall stability; however, the observed occurrences of peeling and cracking in the top and side spray layers necessitate a comprehensive evaluation of its structural stability and integrity.

### On site loose ring testing

The utilization of the RSM-SY7 detector to ascertain the extent of the loose rock zone involved testing the ultrasonic wave velocity at specific measurement points within the DSSC, SCC, and SPTC tunnels. According to the

test findings presented in Fig. 3, at measurement point 1 situated beyond a 3-m radius from the tunnel wall, the ultrasonic wave velocity consistently exceeds 7 km/s, indicative of the excellent integrity of the rock mass in this outer region. Conversely, at measurement points 2 and 3, the relatively intact rock mass lies approximately 2.5 m away from the tunnel wall. Consequently, the loose rock zone within this super large cross-section chamber group is confined within a 3 m radius (corresponding to the maximum recorded value).

**Numerical simulation analysis**  
**Model building**

The engineering example provides a detailed numerical model established in FLAC<sup>3D</sup>, showcasing various parameters and dimensions integral to the simulation process. As shown in Fig. 4, the model features a height of 110 m, with rock layers' thickness tailored to real-world conditions. The model length spans 100 m, with a 44 m distance between the chamber and model boundary, while the spacing between chambers is determined based on simulation requirements. Cuboid elements characterize the model, with dimensions set at 1 m, 2 m, and 4 m, corresponding to the tunnel's proximity. Additionally, the cavern's average depth is specified at 813 m, with the chamber roof positioned 58 m from the model's top boundary. The average bulk density of the overburden rock is recorded at 25,000 N/m<sup>3</sup>, leading to a self-weight stress application of 18.8 MPa on the model's top surface. Displacement constraints are enforced on other model surfaces, with the initial stress field presumed to mirror the equal horizontal and self-weight stresses due to the absence of specific horizontal stress data in the research area.

Notably, the chamber section exhibits a construction comprising a straight wall semi-circular arch design, featuring a section height of 9 m, a straight wall height of 5 m, and a section width measuring 8 m. An intriguing aspect to consider is the chamber's structural composition, with the straight wall segment positioned within the coal seam, while the arched portion is situated within the sandstone layer. To further contextualize the design and operational parameters, the model parameters are outlined in Table 1, reflecting the intricate interplay between geological characteristics and structural considerations.

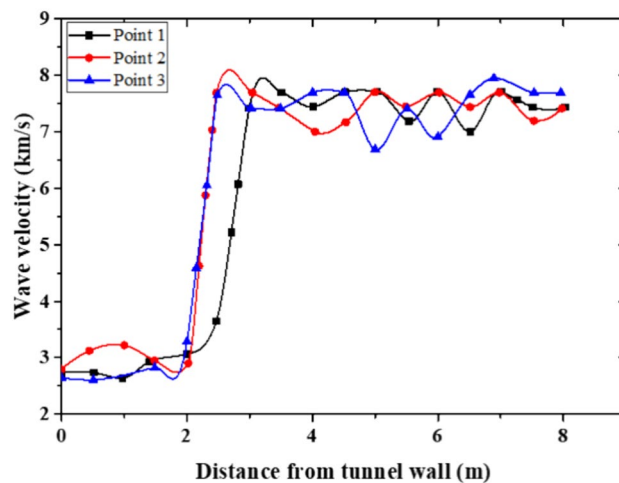


**Figure 3.** Results of ultrasonic wave velocity at each sites.

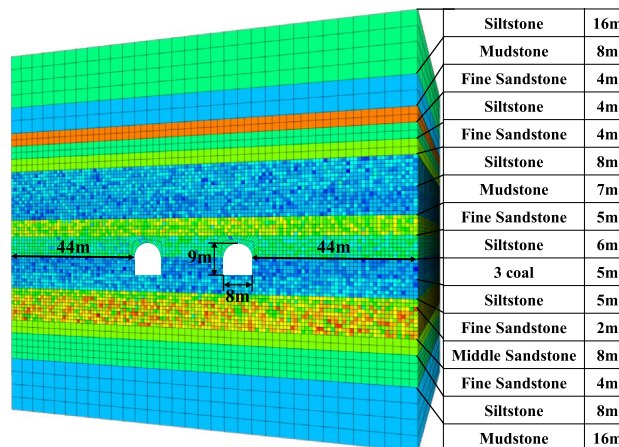


**Figure 4.** Numerical simulation mode.

Lithology	Density (kg/m <sup>3</sup> )	Bulk /GPa	Shear /GPa	Cohesion /MPa	Fiction /°	Tensile /MPa
Coal	1400	2.45	1.51	1.00	28.5	1.00
Siltstone	2630	3.91	3.03	2.50	32	3.15
Fine sandstone	2540	5.87	4.47	4.26	32	4.19
Medium sandstone	2580	6.82	3.69	8.00	24.5	5.15
Mudstone	2210	2.56	1.72	1.55	26	1.58

**Table 1.** Mechanical properties of rocks used in the numerical simulation model<sup>20</sup>.

The model described serves as an essential tool for simulating and analyzing various aspects of the near-field surrounding rock within the context of different tunnel spacing scenarios. Specifically, the stress distribution characteristics, displacement patterns around the tunnel, and identification of potential damage and failure zones are key focal points in this simulation framework. The prescribed spacing configurations entail chamber intervals set at 2.5 times, 2.0 times, and 1.5 times the chamber width, translating to spacings of 20 m, 16 m, and 12 m, respectively. An intriguing feature of the simulation methodology involves a single excavation process on the left chamber, while the right chamber undergoes excavation in increments of 5 m over 20 stages, aligning with practical operational protocols.

### Simulation result analysis

#### Plastic zone range

The visualization provided in Fig. 5 offers valuable insights into the variation in plastic zones across tunnels with differing inter-tunnel spacings. For a specific chamber configuration depicted in Fig. 5a, a comprehensive analysis reveals distinctive characteristics within the plastic zones. Notably, in this scenario, the maximum extent of plastic deformation is observed at the upper and lower regions of the chamber, spanning distances of 3 m and 5 m, respectively. Moving horizontally, the peak range of plastic zone development coincides with the semi-circular arch and straight wall interface, encompassing a distance of 6 m. Within the circular arc section of the chamber, the plastic deformation manifests within a narrower range, spanning from 4 to 5 m.

The observations following the excavation of adjacent chambers offer crucial insights into the evolution of plastic zones within the tunnel system. Notably, the maximum range of plastic deformation at the upper and lower regions of the chamber remains consistent post-excavation, indicating stable conditions in these regions. Similarly, the plastic zone extent on the side of the tunnel opposite to the rock pillar remains unchanged. However, a notable shift is observed as the distance between the chambers decreases, leading to a gradual development of the plastic zone parallel to the straight wall on this side.

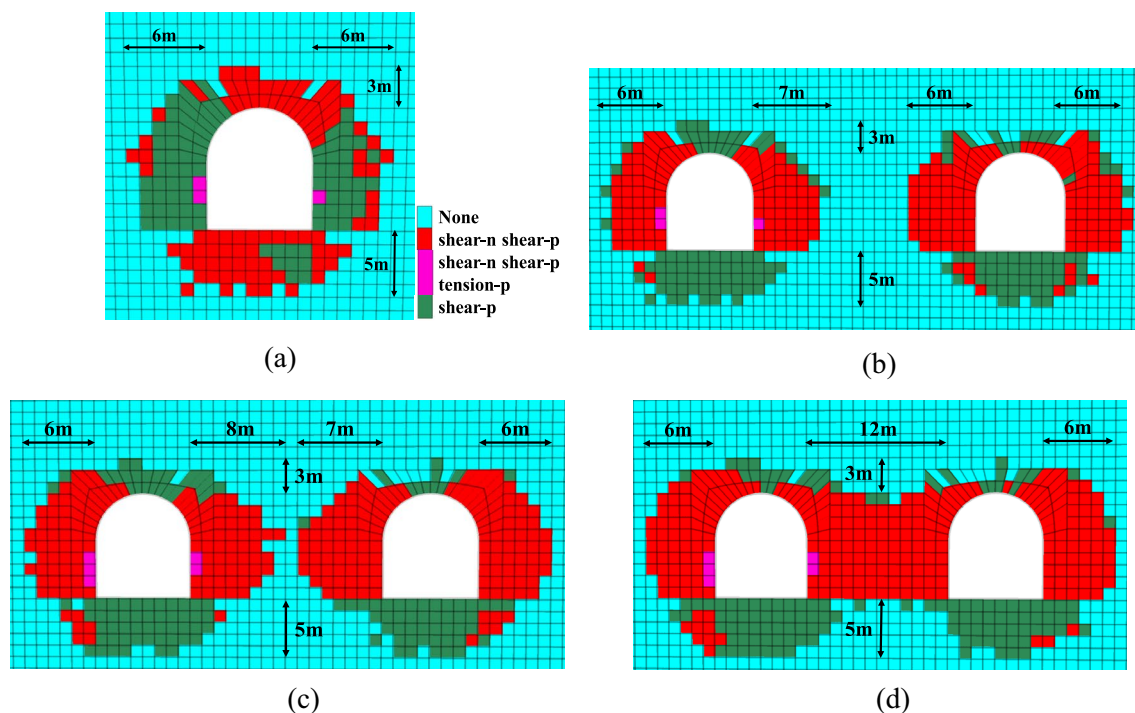


**Figure 5.** The plastic zone under different spacing.

As the inter-chamber spacing decreases, the plastic zone gradually expands, impacting the integrity of the rock column. For instance, with a spacing of 20 m, the total plastic zone coverage on both sides is 13 m, retaining a 7 m undamaged area in the rock column. When this spacing reduces to 16 m, the plastic zone's total coverage increases to 15 m, leaving only a 1 m undamaged area in the rock column. Further reduction to a 12 m spacing engulfs the entire rock column within the plastic zone. Consequently, it is advisable to implement timely support measures and monitoring protocols to mitigate risks associated with plastic zone expansion.

The analysis underscores the importance of maintaining a minimum spacing between chambers equivalent to 1.5 times the chamber width in super large cross-section chamber groups within mining operations, ensuring structural stability, risk mitigation, and operational safety in complex underground environments.

#### *Stress state of surrounding rock*

The arrangement of monitoring points within the numerical model, as depicted in Fig. 6, plays a pivotal role in capturing and analyzing crucial data related to stress distribution and displacement patterns in the tunnel structure. Specifically, the monitoring point layout includes provisions for monitoring patterns and displacement along the horizontal line, as well as tracking displacement along the vertical line.

The stress analysis conducted on the rock column within the chambers underscores the evolving patterns of tangential stress and radial stress based on variations in inter-chamber spacing. The tangential stress distribution within the rock column exhibits noteworthy variations across different spacing configurations (see Fig. 7). In a scenario with a 20 m spacing between chambers, the maximum tangential stress registers at 38.27 MPa, reflecting an increase compared to the single-chamber setting. Conversely, as the spacing reduces to 16 m, the maximum tangential stress escalates to 47.02 MPa, indicating heightened stress levels and potential instability within the rock column.

In the case of a 12 m inter-chamber spacing, the tangential stress gradient intensifies from the chamber wall towards the center of the rock column, reaching a peak of 37.88 MPa. This elevated stress concentration signifies an increased risk of instability and structural failure within the rock column, necessitating proactive risk mitigation measures and structural reinforcement strategies to ensure operational safety and tunnel integrity.

It is essential to carefully monitor the tangential stress distribution and fluctuations within the rock column, particularly in regions prone to high stress concentrations, to preemptively identify areas at risk of failure and implement targeted interventions to enhance the stability and resilience of the tunnel system in response to dynamic stress environments.

The findings from the analysis indicate a clear correlation between the excavation of adjacent chambers and the escalation of maximum tangential stress within the rock column. As the spacing between chambers diminishes, there is a progressive increase in tangential stress levels, reflecting heightened mechanical loading and potential structural vulnerabilities. However, an intriguing observation emerges when the chamber spacing is reduced to a critical threshold: the tangential stress fails to attain its peak value, signaling a deviation from the anticipated stress intensification trend and hinting at the onset of structural instability within the rock column.

#### *Displacement of rock pillar support*

The radial displacement analysis of the rock column in the chamber configuration highlights crucial insights into the deformation patterns and displacement magnitudes based on varying inter-chamber spacing (see Fig. 8). The displacement profiles reveal distinctive changes in the magnitude and distribution of radial displacements along the tunnel walls, illustrating the influence of chamber proximity on rock mass behavior and stability.

In the case of a 20 m spacing between chambers, the radial displacement distribution exhibits a notable increase in the maximum displacement values on both the left and right chamber walls compared to the single-chamber excavation scenario. The spatial distribution of displacements indicates a concentration of significant displacements within the plastic zone of the rock column, especially within a 6 m range from the tunnel wall, emphasizing the localized deformation effects attributed to excavation activities and stress redistribution processes.

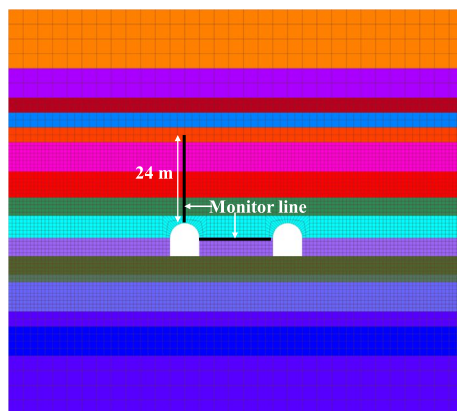


**Figure 6.** Location of the monitoring point arrangement in the numerical model.

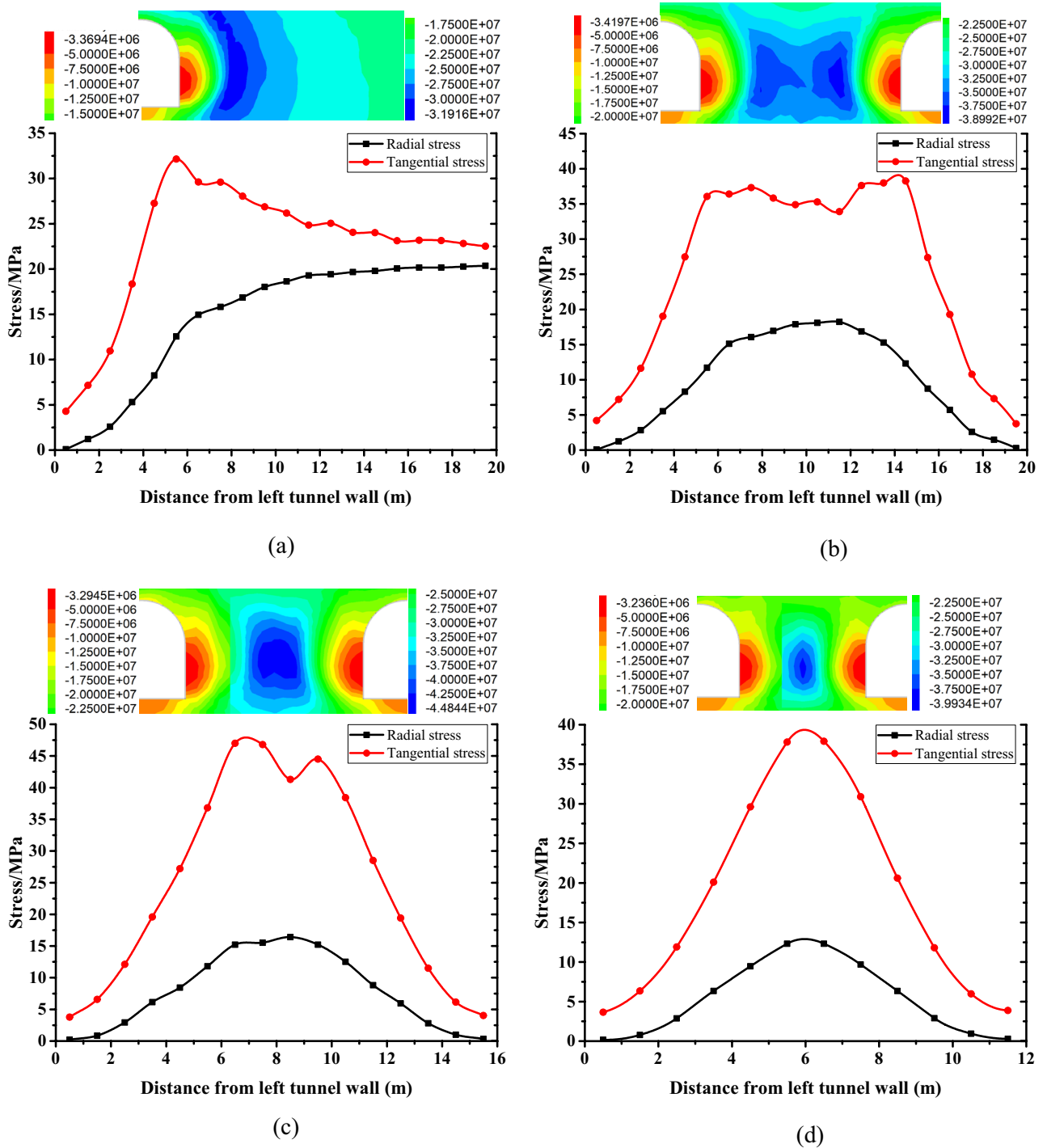


**Figure 7.** The stress state of the surrounding rock under different spacing.

As the chamber spacing decreases to 16 m, there is a further escalation in the maximum displacement values observed on the chamber walls, accompanied by an expansion of the plastic zone within the rock column. The displacement cloud map highlights areas of relatively low displacement, particularly in the trapezoidal region at the base of the rock column, offering valuable insights into deformation characteristics and stress distribution patterns within the chamber configuration.

Upon reducing the spacing between chambers to 12 m, a pronounced increase in the maximum displacement values is recorded, signifying heightened deformation in the rock mass surrounding the chambers. The emergence of a small triangular area with relatively lower displacements at the bottom of the rock column underscores the complex interplay between excavation-induced stresses, rock mass response, and structural stability considerations in underground chamber layouts.

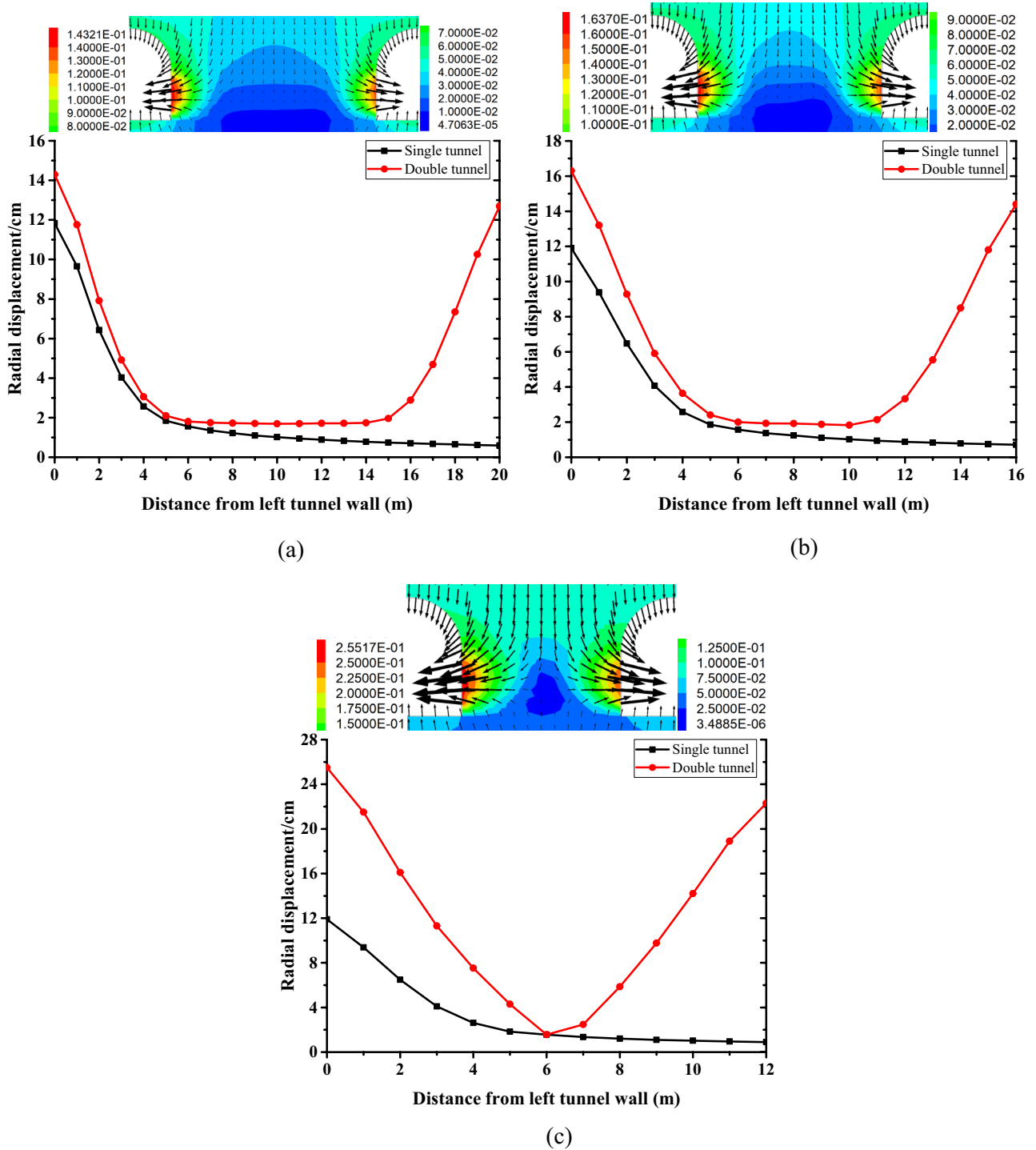


**Figure 8.** The displacement of rock pillar under different spacing.

*Top displacement of the chamber*

The radial displacement curves depicting the chamber roof under varying spacing conditions are illustrated in Fig. 9. In cases where a single chamber is considered, the region experiencing substantial displacement on the chamber roof is confined within a 2-m radius. However, as the excavation progresses towards the adjacent chamber, there is a noticeable surge in roof displacement as the inter-chamber distance diminishes. Specifically, for inter-chamber spacings of 20 m, 16 m, and 12 m, the displacement on the chamber roof increments by approximately 1.5 cm, 2.0 cm, and 4.2 cm, respectively, when compared to that of a solitary chamber. Notably, when the chamber separation is set at 16 m, the displacement extends beyond the peak displacement seen in single-chamber scenarios within the 12 m zone above the chamber roof. Furthermore, under 12 m chamber spacing, the chamber roof displacement intensifies considerably, signifying heightened instability. Consequently,

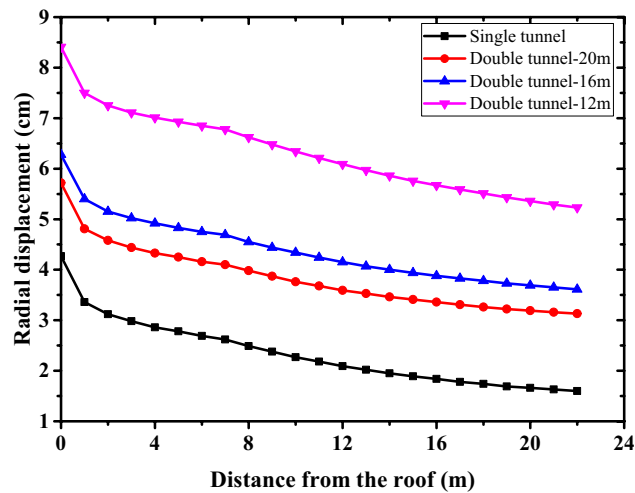


**Figure 9.** The displacement of chamber roof area under different spacing.

under these two spacing configurations, there exists an elevated risk of cave roof collapse, underscoring the critical importance of proactive measures to ensure structural stability and safety during underground excavations.

Based on the aforementioned displacement analysis, it is evident that with the sequential excavation of adjacent chambers, the displacement within the immediate perimeter of the surrounding rock progressively escalates. Moreover, the displacement around the initially excavated chamber marginally surpasses that of the subsequent excavation. This phenomenon highlights a gradual augmentation in chamber roof displacement, thereby amplifying the looming threat of collapse. Furthermore, examination of the displacement cloud map reveals that the lower segment of the rock column manifests as a stable region amidst the evolving displacement dynamics in the vicinity. This delineation underscores the spatial variations in displacement magnitudes and emphasizes the criticality of assessing and mitigating potential instabilities to ensure the structural integrity and safety of underground excavations.

#### *Qualitative discussion on surrounding rock areas*

Building on the simulation analysis and in conjunction with the outcomes from on-site loose ring testing, the rock column can be segmented into distinct zones, as exemplified in Fig. 10. The initial segment encompasses the broken zone, characterized by a substantial decrement in the sound wave velocity of the rock mass. This region represents a significantly damaged domain that poses a high risk of chamber roof collapse or rock pillar instability. The subsequent portion denotes the loose zone, constituting a plastic zone encompassing regions beyond the broken zone. Within this realm, there is a progressive increase in the sound wave velocity of the rock mass. Nonetheless, the absence of effective tunnel support in this sector could precipitate secondary tunnel impairments. Predominantly, the middle areas can be classified as stable zones, offering a sense of structural robustness. Notably, the trapezoidal segment beneath the midsection of the rock column can be delineated as

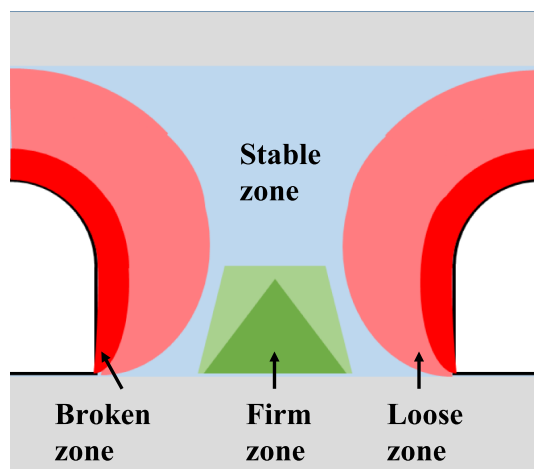


**Figure 10.** Damage area division of rock pillar.

a firm zone, denoting a restoration of the rock mass’s sound wave velocity to normalcy. Noteworthy dynamics arise as the inter-chamber spacing diminishes, where the broken and loose zones expand proportionally, the stable zone gradually contracts, and eventually diminishes, while the firm zone transitions from a trapezoidal configuration to a triangular layout. Upon reaching critically small chamber spacings, the rock pillars are at risk of instability and comprehensive failure as an entirety. This delineation of zones underscores the imperative nature of meticulously evaluating and addressing potential instabilities to safeguard the structural integrity and operational resilience of underground excavations.

### Failure criteria for double chambers

Given the premise that the rock mass adheres to the Mohr–Coulomb criterion and functions as an ideal plastic body, with the coefficient of lateral pressure  $\lambda$  set at 1, the original stress of the rock is denoted as  $P_0$ , while the chamber radius is represented by  $r_a$ . And the plastic zone radius of a single circular chamber after excavation is (see the appendix)<sup>35</sup>:

$$R_p = r_a \left[ \frac{2p_0(\xi - 1) + 2\sigma_c}{\sigma_c(\xi + 1)} \right]^{\frac{1}{\xi - 1}} \tag{1}$$

where,  $\xi = \frac{1 + \sin \varphi}{1 - \sin \varphi}$ ,  $\xi = \frac{2c \cdot \cos \varphi}{1 - \sin \varphi}$ .

For non-circular chambers, the equivalent radius method is used to equate the chamber radius. The basic principle of the equivalent radius method is to simplify a non-circular underground chamber with a virtual circle, whose area is equal to the cross-sectional area of the non-circular underground chamber. The virtual circle radius is corrected by multiplying it by the corresponding coefficient, as shown in Eq. (2)<sup>36</sup>:

$$r^{eq} = k \cdot (S/\pi)^{1/2} \tag{2}$$

where,  $S$  is the actual cross-sectional area of the non-circular underground chamber,  $m^2$ ;  $r^{eq}$  is the “equivalent radius” of a non-circular underground chamber,  $m$ ;  $k$  is the correction coefficient, and for arched tunnels,  $k$  is 1.1<sup>36</sup>. Therefore, the equivalent plastic zone radius for a single non circular chamber is:

$$R_p^{eq} = k \cdot (S/\pi)^{1/2} \left[ \frac{2p_0(\xi - 1) + 2\sigma_c}{\sigma_c(\xi + 1)} \right]^{\frac{1}{\xi - 1}} \tag{3}$$

According to Eq. (2), the equivalent radius in the above simulation model is approximately 5.0 m. Due to the fact that the arched part of the tunnel is located in the siltstone layer and the straight wall part is located in the coal seam, their respective parameters are introduced into formula (3), and their plastic equivalent radii are obtained to be 8.0 m and 13.4 m, respectively. According to the proportion of the cross-section area of the tunnel in each rock layer, the equivalent plastic radius is obtained to be 11.3 m. The maximum range of its plastic zone is approximately 6 m, which is consistent with the simulation results.

Based on the aforementioned simulation results, it can be inferred that in the case of two parallel excavated chambers, if the separation distance between them is sufficiently large, they can attain an equilibrium state independently without mutual interference. Conversely, as the spacing between the chambers decreases incrementally, the excavation process in one chamber begins to impact the elastic zone of the adjacent chamber, leading to alterations in stress distribution and rock pillar displacement. Consequently, a portion of the elastic zone undergoes a transition into a plastic zone, as visually depicted in Fig. 11. Owing to the interplay between the two

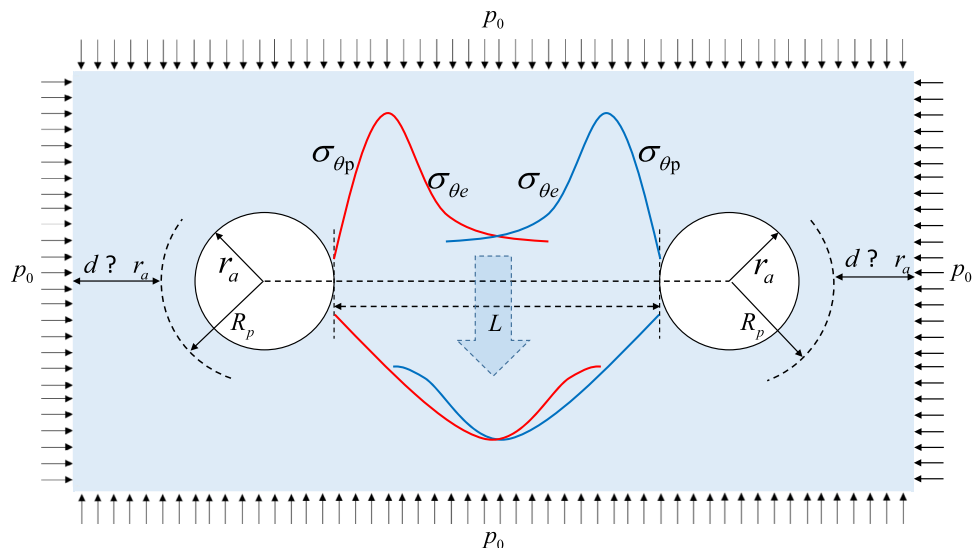


**Figure 11.** Stress distribution in parallel chambers.

chambers, the original boundary of the plastic zone progressively converges towards the midpoint between the chambers. Subsequently, when the spacing between the chambers diminishes significantly, the boundaries of their respective plastic zones tend to overlap, indicating that the rock column is situated within the plastic zone and becomes susceptible to instability and potential failure.

From the above simulation analysis, it can be concluded that the spacing between chambers should not be less than 1.5 times the width of the chambers. When the distance between two chambers is twice the width of the chamber, the boundaries of the two plastic zones basically intersect, which can be used as the minimum reasonable chamber distance. And this distance is approximately the width of two plastic zones plus one chamber radius:

$$L = 2(R_p^{eq} - r^{eq}) + r^{eq} = 2R_p^{eq} - r^{eq} \quad (4)$$

By substituting Eqs. (2) and (3) into the above equation, we can obtain

$$L = k \cdot (S/\pi)^{1/2} \left( 2 \left[ \frac{2p_0(\xi - 1) + 2\sigma_c}{\sigma_c(\xi + 1)} \right]^{\frac{1}{\xi-1}} - 1 \right) \quad (5)$$

Formula (5) can be used as a criterion for the failure of double chambers. If it is necessary to excavate a tunnel within this distance, it is recommended to provide timely support, improve the support strength, and conduct monitoring to identify potential safety hazards.

Using the coal gangue separation system at Longgu Coal Mine as a case study to validate the usability of Eq. (5). It is observed that the arched section of the chamber is situated within the siltstone layer, while the straight wall section aligns with the coal seam. By incorporating the respective parameters into formula (5), the calculated minimum spacings between the chambers are determined to be 11.0 m and 21.8 m. Additionally, based on the cross-sectional area proportions of the tunnel within each rock layer, the derived minimum spacing is 17.62 m. During the practical implementation phase, the chosen minimum spacing was established at 14.75 m, resulting in the adoption of a united timbering system comprising bolt-net-tightwire reinforcement combined with concrete spraying for tunnel support. Presently, the overall stability of the tunnel network is satisfactory; however, some instances of peeling and cracking in the upper layers of the tunnel are evident (refer to Fig. 12). These occurrences indirectly validate the relevancy and effectiveness of Eq. (5) in assessing and managing the structural stability challenges encountered during construction.

To be honest, the support condition is not considered. In the time sequence, the support is after excavation. Significantly, the stress equilibrium of the surrounding rock undergoes alterations. The primary role of support lies in averting the collapse and descent of fractured rock masses. In contrast to the elevated crustal stress and stress focalization induced by excavation activities, the impact of support on the stress distribution within the adjacent rock mass is deemed inconsequential. Hence, the consideration of support influence was omitted. Validating the formula through the utilization of supported chambers presents a viable proposition to affirm its efficacy.

## Conclusion

This study focuses on the large cross-section chamber group within the underground coal gangue separation system. It systematically examines the deformation, failure range, and stress state of the surrounding rock. The analysis culminates in the following conclusions.

1. When the spacing between chambers is less than 2.0 times the width of the chamber, there is a significant increase in the extent of the plastic zone. Notably, when the spacing between chambers equals 1.5 times the width of the chambers, the entirety of the rock column falls within the plastic zone range. A decrease in chamber spacing correlates with heightened tangential stress levels within the rock pillar range. Specifically,

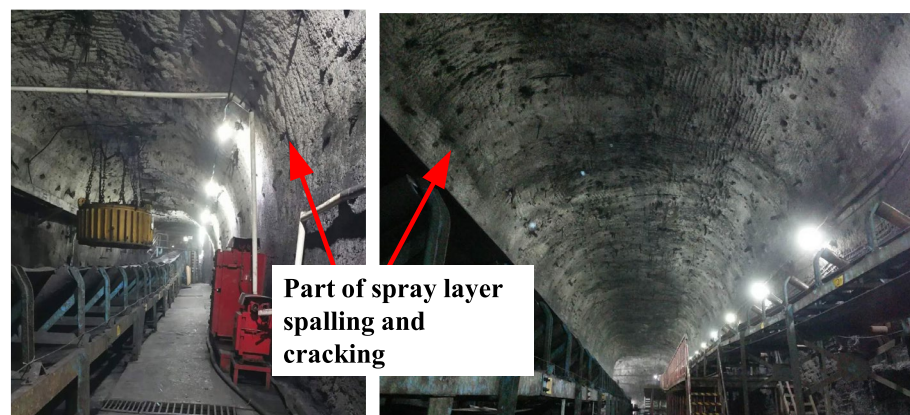


**Figure 12.** Photographs of chamber surrounding rock.

- for spacing ratios of 2.5, 2.0, and 1.5 times the chamber width, the maximum tangential stresses are recorded at 1.19, 1.46, and 1.18 times that of a single chamber, respectively.
- As the spacing between chambers diminishes, there is a notable escalation in displacement on both sides of the rock column and the chamber roof. Furthermore, the displacement surrounding the initially excavated chamber marginally exceeds that of subsequently excavated chambers. Through a comprehensive integration of plastic zone delineation and stress analysis, the rock mass proximate to the rock pillar is categorized into four distinct zones: the fracture zone, loose zone, stable zone, and compact zone. Notably, with decreasing chamber spacing, the stable zone progressively vanishes, leading to a contraction of the compact zone into a triangular configuration at the base of the central rock pillar.
  - An approximate solution for determining the plastic zone boundary of non-circular chambers has been introduced, demonstrating consistency with numerical simulation outcomes. Through numerical simulations involving double chambers, a minimum acceptable chamber spacing has been established. This spacing threshold serves as a pivotal criterion for assessing the potential failure of double chambers.

The findings hold significant guiding implications for determining the optimal minimum spacing between adjacent super large section chambers and ensuring the stability of these chambers, particularly in the context of mine excavations.

### Data availability

The data used to support the findings of this study are available from the corresponding author upon request.

Received: 15 May 2024; Accepted: 15 July 2024

Published online: 22 July 2024

### References

- Hao, Y. *et al.* An innovative equivalent width supporting technology for sustaining large-cross section roadway in thick coal seam. *Arab. J. Geosci.* **12**(22), 1–12 (2019).
- Li, M., Aminossadati, S. M. & Wu, C. Numerical simulation of air ventilation in super-large underground developments. *Tunn. Undergr. Sp. Tech.* **52**, 38–43 (2016).
- Meng, B. *et al.* Failure mechanism and stability control of a large section of very soft roadway surrounding rock shear slip. *Int. J. Min. Sci. Technol.* **23**(1), 127–134 (2013).
- Li, C. *et al.* Mechanism and practice of rock control in deep large span cut holes. *Min. Sci. Technol.* **21**(6), 891–896 (2011) ((in Chinese)).
- Gao, M. Z. *et al.* Study on in-situ disturbed mechanical behavior of deep coal rock. *J. China Coal Soc.* **45**(08), 2691–2703 (2020) ((in Chinese)).
- Zhang, C., Canbulat, I., Hebblewhite, B. & Ward, C. R. Assessing coal burst phenomena in mining and insights into directions for future research. *Int. J. Coal Geol.* **179**, 28–44 (2017).
- Konicek, P., Soucek, K., Stas, L. & Singh, R. Long-hole destress blasting for rockburst control during deep underground coal mining. *Int. J. Rock Mech. Min. Sci.* **61**, 141–153 (2013).
- Liu, J. X. *et al.* High-stress chamber stability in kilometer-deep coal mines: A case study. *Geotech. Geol. Eng.* **42**(4), 2425–2438 (2024).
- Li, G. *et al.* A new elastic–plastic analytical solution of circular tunnel under non-axisymmetric conditions. *Sci. Rep.-UK* **12**(1), 1–20 (2022).
- Yunliang, T. *et al.* Discrimination method and engineering characteristics of super large section chamber in coal mine. *J. Min. Saf. Eng.* **1**, 23–31 (2020) ((in Chinese)).
- Wang, M. Y., Zhang, N., Li, J., Ma, L. J. & Fan, P. X. Computational method of large deformation and its application in deep mining tunnel. *Tunn. Undergr. Sp. Tech.* **50**, 47–53 (2015).
- Deng, S. X., Li, J., Jiang, H. M. & Wang, M. Y. Experimental and theoretical study of the fault slip events of rock masses around underground tunnels induced by external disturbances. *Eng. Geol.* **233**, 191–199 (2018).
- Mohammad, R. Z. & Ahmad, F. Analytical solutions for the stresses and deformations of deep tunnels in an elastic-brittle-plastic rock mass considering the damaged zone. *Tunn. Undergr. Sp. Tech.* **58**, 186–196 (2016).
- Hou, X. Elasto-plastic theory of the underground circular structure. *J. Tongji Univ. Nat. Sci.* **10**(4), 50–62 (1982) ((in Chinese)).
- Wang, H. N. *et al.* Analytical stress and displacement due to twin tunneling in an elastic semi-infinite ground subjected to surcharge loads. *Int. J. Numer. Anal. Met.* **2018**, 1 (2018).
- Chen, Z. *Analytical Method in Mechanical Analysis of Surrounding Rock* (China Coal Industry Publishing House, 1983) ((in Chinese)).
- Lu, A., Zhang, N. & Qin, Y. Analytical solutions for the stress of a lined non-circular tunnel under full-slip contact conditions. *Int. J. Rock. Mech. Min.* **79**, 183–192 (2015).
- Li, Y. & Chen, S. A complex variable solution for lining stress and deformation in a non-circular deep tunnel II practical application and verification. *Math. Comput. Appl.* **23**(43), 1–14 (2018).
- Zhang, L., Yang, Z. & Li, X. The development of rock mechanics and Engineering in the new century-Proceedings of the Sixth Academic Conference of Chinese society of rock mechanics and Engineering. In *Beijing: China Academic Journal of Electronic Publishing House* 671–674 (2000) (in Chinese).
- Wang, J., Ning, J. G., Qiu, P. Q., Yang, S. & Shang, H. F. Microseismic monitoring and its precursory parameter of hard roof collapse in longwall faces: A case study. *Geomech. Eng.* **17**(4), 375–383 (2019).
- Wang, J., Ning, J. G., Jiang, J. Q. & Bu, T. T. Structural characteristics of strata overlying of a fully mechanized longwall face: A case study. *J. S. Afr. I. Min. Metall.* **118**, 1195–1204 (2018).
- Wen, Z. J., Xing, E. R., Shi, S. S. & Jiang, Y. J. Overlying strata structural modeling and support applicability analysis for large mining-height stopes. *J. Loss Prevent Proc.* **57**, 94–100 (2019).
- Fan, D., Liu, X., Tan, Y., Li, X. & Purev, L. Instability energy mechanism of super-large section crossing chambers in deep coal mines. *Int. J. Min. Sci. Technol.* **32**(5), 1075–1086 (2022).
- Liu, X. *et al.* Failure evolution and instability mechanism of surrounding rock for close-distance parallel chambers with super-large section in deep coal mines. *Int. J. Geomech.* **5**, 21 (2021).
- Xie, S. *et al.* Failure analysis and control technology of intersections of largescale variable crosssection roadways in deep soft rock. *Int. J. Coal Sci. Technol.* **9**(2), 124–146 (2022).

26. Li, S. C. *et al.* Study on mechanism of macro failure and micro fracture of local nearly horizontal stratum in super-large section and deep buried tunnel. *Geomech. Eng.* **11**(2), 253–267 (2016).
27. Jiang, F., Huang, D. & Liao, C. Cavern group layout of underground powerhouse of a hydropower station. *Design Hydroelectr. Power Station* **21**(2), 8–10 (2005) ((in Chinese)).
28. Tan, Y. *et al.* Numerical investigation of failure evolution for the surrounding rock of a super-large section chamber group in a deep coal mine. *Energy Sci. Eng.* **7**, 3124–3146 (2019).
29. Yang, Y. *et al.* Analysis of construction parameter optimization for new large cross-section tunnel next to existing tunnels. *Rock Soil Mech.* **31**(4), 1217–1226 (2010) ((in Chinese)).
30. Liu, X. *et al.* Similar simulation study on the deformation and failure of surrounding rock of a large section chamber group under dynamic loading. *Int. J. Min. Sci. Technol.* **31**(3), 495–505 (2021).
31. Qi, K., Tan, Z. Y. & Li, W. Stability analysis on the crossed cavern group in underground mine. *Min. R. D.* **37**, 52–55 (2017).
32. Lin, H. L. & Shi, Y. K. Simulation on stability of surrounding rock of large section chambers in deep structural complex areas. *J. China Coal Soc.* **36**, 1619–1623 (2011) ((in Chinese)).
33. Li, W. T. *et al.* An improved numerical simulation approach for arch-bolt supported tunnels with large deformation. *tunn. Undergr. Sp. Tech.* **77**, 1–12 (2018).
34. Li, W. T. *et al.* Mechanism and control of failure of rock roadway support in highly stressed soft rock. *Chin. J. Rock Mech. Eng.* **34**, 1836–1848 (2015) ((in Chinese)).
35. Shen, M. & Chen, J. *Rock mechanics* 153–159 (Tongji University Press, 2006).
36. Liu, C., Cao, L. & Liu, S. Method of “Equivalent Radius” for the analyzing rock stress of high-buried non-circular underground chambers. *Copper Eng.* **1**, 1–5 (2010) ((in Chinese)).

## Acknowledgements

This work was supported by the National Natural Science Foundation of China (52104135) and the Natural Science Foundation of Shandong Province (ZR2021QE213).

## Author contributions

Zihui Wang wrote the main manuscript. Shuo Zhang did the simulation work. Deyuan Fan modified the paper. Dongxiao Zhang revised the manuscript.

## Competing interests

The authors declare no competing interests.

## Additional information

**Supplementary Information** The online version contains supplementary material available at <https://doi.org/10.1038/s41598-024-67711-5>.

**Correspondence** and requests for materials should be addressed to D.Z.

**Reprints and permissions information** is available at [www.nature.com/reprints](http://www.nature.com/reprints).

**Publisher’s note** Springer Nature remains neutral with regard to jurisdictional claims in published maps and institutional affiliations.



**Open Access** This article is licensed under a Creative Commons Attribution-NonCommercial-NoDerivatives 4.0 International License, which permits any non-commercial use, sharing, distribution and reproduction in any medium or format, as long as you give appropriate credit to the original author(s) and the source, provide a link to the Creative Commons licence, and indicate if you modified the licensed material. You do not have permission under this licence to share adapted material derived from this article or parts of it. The images or other third party material in this article are included in the article’s Creative Commons licence, unless indicated otherwise in a credit line to the material. If material is not included in the article’s Creative Commons licence and your intended use is not permitted by statutory regulation or exceeds the permitted use, you will need to obtain permission directly from the copyright holder. To view a copy of this licence, visit <http://creativecommons.org/licenses/by-nc-nd/4.0/>.

© The Author(s) 2024